Mesonic and nonmesonic weak decay widths of medium-heavy Λ hypernuclei

Y. Sato,[1,3] S. Ajimura,[5] K. Aoki,[3] H. Bhang,[2] T. Hasegawa,[4,*] O. Hashimoto,[1] H. Hotchi,[4,†] Y. D. Kim,[2,3,‡] T. Kishimoto,[5] K. Maeda,[1] H. Noumi,[3] Y. Ohta,[4] K. Omata,[3] H. Outa,[3] H. Park,[2] M. Sekimoto,[3] T. Shibata,[3] T. Takahashi,[1,3] and M. Youn[2,3]

[1]*Department of Physics, Tohoku University, Sendai 980-8578, Japan*

[2]*Department of Physics, Seoul National University, Seoul 151-742, Korea*

[3]*High Energy Accelerator Research Organization (KEK), Tsukuba, Ibaraki 305-0801, Japan*

[4]*Graduate School of Science, University of Tokyo, Tokyo 113-0033, Japan*

[5]*Department of Physics, Osaka University, Toyonaka, Osaka 560-0043, Japan*

(Received 13 April 2003; revised manuscript received 2 June 2004; published 9 February 2005)

We have measured the energy spectra of pions and protons emitted in the weak decay of ${}^{12}_{\Lambda}$C, ${}^{28}_{\Lambda}$Si, and ${}_{\Lambda}$Fe hypernuclei produced via the (π^+, K^+) reaction. The decay widths of the π^- mesonic decay ($\Lambda \to p\pi^-$) and the nonmesonic decay ($\Lambda N \to NN$) were extracted. The present results demonstrate an increase of the mesonic decay width due to a distortion of the pion wave function in nuclear medium for the first time. The ratios of the neutron- to proton-induced nonmesonic decay widths, $\Gamma_n(\Lambda n \to nn)/\Gamma_p(\Lambda p \to np)$, were evaluated by a direct comparison of the measured proton energy spectra with the calculated ones. No theoretical calculation which has been proposed so far can simultaneously account for both the nonmesonic decay widths and the Γ_n/Γ_p ratios in the present data.

DOI: 10.1103/PhysRevC.71.025203 PACS number(s): 21.80.+a, 13.30.Eg, 13.75.Ev, 21.10.Tg

I. INTRODUCTION

The Λ hypernuclei have been extensively studied since their first discovery in a nuclear emulsion [1]. A Λ hyperon, which carries a degree of freedom, "strangeness," can be used as a unique probe to investigate the interior of the nucleus because it does not suffer from the Pauli exclusion principle.

A Λ hypernucleus is usually produced in an excited state of a Λ-particle neutron-hole configuration. When a Λ hypernucleus is excited above the particle emission threshold, it decays dominantly by the strong interaction and then deexcites to its ground state via electromagnetic transitions. From the ground state, it eventually decays through the weak interaction.

The total decay width ($\Gamma_{\rm tot} = 1/\tau_{HY}$) of a Λ hypernucleus is composed of the mesonic decay width (Γ_m) and the nonmesonic decay width (Γ_{nm}). In the mesonic decay, a Λ hyperon decays into a nucleon and a pion in the nuclear medium, similarly as in free space. The mesonic decay width (Γ_m) can be further expressed as a sum of the decay widths for emitting negative ($\Gamma_{\pi^-} : \Lambda \to p\pi^-$) and neutral ($\Gamma_{\pi^0} : \Lambda \to n\pi^0$) pions, respectively. In two-body nonmesonic decay, however, a Λ hyperon in a nucleus interacts with a neighboring nucleon and decays into a pair of nucleons without emitting a pion. The nonmesonic decay width (Γ_{nm}) is composed of the proton-induced ($\Gamma_p : \Lambda p \to np$) and neutron-induced ($\Gamma_n : \Lambda n \to nn$) decay widths. In addition, the importance of the two nucleon-induced decay width ($\Gamma_{2N} : \Lambda NN \to NNN$) has also been discussed theoretically [2], although it has not been experimentally established yet.

Therefore, the lifetime (τ_{HY}), the total ($\Gamma_{\rm tot}$) and partial decay widths of Λ hypernuclei are connected by the following relationship,

$$1/\tau_{HY} = \Gamma_{\rm tot} = \Gamma_m + \Gamma_{nm}, \quad (1)$$

$$\Gamma_m = \Gamma_{\pi^-} + \Gamma_{\pi^0}, \quad (2)$$

$$\Gamma_{nm} = \Gamma_p + \Gamma_n (+\Gamma_{2N}). \quad (3)$$

The mesonic decay releases energy of $Q^{\rm free} \simeq 40$ MeV, corresponding to a momentum of about 100 MeV/c in the center-of-mass system (c.m.) for the emitted nucleon and pion. Because this is much smaller than the nuclear Fermi momentum ($k_F \sim 270\,{\rm MeV}/c$) in typical nuclei, except for light ones, the mesonic decay is strongly suppressed in heavier hypernuclei due to the Pauli exclusion principle acting on the nucleon in the final state.

Although there are several experimental data of Γ_{π^-} and/or Γ_{π^0} on light Λ hypernuclei, such as ${}^{4}_{\Lambda}$H [3], ${}^{4}_{\Lambda}$He [4], ${}^{5}_{\Lambda}$He [5], ${}^{11}_{\Lambda}$B, and ${}^{12}_{\Lambda}$C [5–7], no finite value has been reported for the mesonic decay widths of Λ hypernuclei heavier than ${}^{12}_{\Lambda}$C. It has been pointed out that the mesonic decay widths are sensitive to the nuclear structure in the final state and the choice of the pion-nucleus optical potentials [8–10]. Although the pion-nucleus potentials have been studied so far through π-nucleus scattering experiments and measurements of x rays from the pionic atoms, the study of mesonic weak decay offers a unique opportunity to investigate pion wave functions deep inside a nucleus, where the Λ hypernuclear weak decay occurs. Therefore, precise and systematic measurements of the mesonic decay widths are long awaited.

Nonmesonic weak decay provides a unique opportunity to study both the parity-conserving and parity-violating terms

*Present address: School of Allied Health Sciences, Kitazato University, Sagamihara 228-8555, Japan.

†Present address: Research Center for Physics and Mathematics, Osaka Electro-Communication University, Neyagawa, Osaka 572-8530, Japan.

‡Present address: Department of Physics, Sejong University, Seoul 143-747, Korea.

in the baryon-baryon weak interaction, which are difficult to experimentally investigate by other means, because the weak component of nucleon-nucleon scattering is usually masked by the strong interaction.

In nonmesonic decay of a Λ hypernucleus, the released energy is $Q^{\text{free}} \simeq 176$ MeV, and the c.m. momentum of two nucleons in the final state is about 400 MeV/c. Because the momentum transfer is larger than the Fermi momentum, the nonmesonic decay does not suffer from Pauli blocking so seriously. Therefore, it dominates over the mesonic decay, except in very light Λ hypernuclei.

Currently, there is no clear picture concerning the nonmesonic decay, although various experimental and theoretical efforts have been attempted for a long time. Nonmesonic decay width (Γ_{nm}), the neutron- and proton-induced partial decay widths (Γ_n and Γ_p), and their ratio (Γ_n/Γ_p) are thought to be good experimental observables.

The lifetimes and partial decay widths of several spin-isospin saturated Λ hypernuclei were measured at Brookhaven National Laboratory (BNL) and the High Energy Accelerator Research Organization (KEK) ($^{5}_{\Lambda}$He [5], $^{11}_{\Lambda}$B, and $^{12}_{\Lambda}$C [5–7]). It was reported that the Γ_n/Γ_p ratios were close to unity or larger, although the quoted errors were large. Contrary to the experimental data, theoretical calculations based on the framework of meson exchange models, assuming the $|\Delta I| = 1/2$ rule, yield Γ_n/Γ_p ratios much smaller than unity (typically 0.1–0.3) [11–13]. The smallness of the Γ_n/Γ_p ratios essentially comes from the tensor dominance of one-pion exchange, which contributes only to the proton-induced nonmesonic decay. The inclusion of the $2\pi/\rho$ exchange processes was discussed in an attempt to cancel out the strong tensor dominance of one-pion exchange potential [14]. Another approach based on the direct quark current exchange has also been suggested to take the short-range nature of the nonmesonic decay and the violation of the $|\Delta I| = 1/2$ rule into account [15]. All of these efforts still resulted in small Γ_n/Γ_p ratios. Good experimental data are seriously required to reveal the mechanism of the nonmesonic decay.

We carried out an experiment to measure the precise lifetimes and partial decay branching ratios of $^{12}_{\Lambda}$C, $^{28}_{\Lambda}$Si, and $_{\Lambda}$Fe hypernuclei produced via the (π^+, K^+) reaction (KEK-PS E307). Because the contribution of mesonic decay to the total decay width becomes smaller, measurements of the nonmesonic decay widths becomes less ambiguous in heavier Λ hypernuclei. The results of lifetime measurements in the present experiment have already been published elsewhere [16,17]. The present article reports results for the π^- mesonic decay widths (Γ_{π^-}), the total nonmesonic decay widths (Γ_{nm}), and the Γ_n/Γ_p ratios of $^{12}_{\Lambda}$C, $^{28}_{\Lambda}$Si, and $_{\Lambda}$Fe hypernuclei, a part of which has already been published in Ref. [18].

The experimental setup is described in Sec. II. The data analysis and results are explained in Sec. III and discussed along with previous studies in Sec. IV. The conclusion is described in Sec. V.

II. EXPERIMENT

The Λ hypernuclei produced by the (π^+, K^+) reaction were identified in the hypernuclear mass spectrum reconstructed using the momenta of the incident pions and the outgoing kaons. The charged particles emitted in the weak decay were detected by the decay counter systems located above and below the experimental target in coincidence with kaons. The branching ratios of the π^- mesonic decay were obtained as ratios between the numbers of identified Λ hypernuclei and pions emitted after the mesonic decay. The π^- mesonic decay width (Γ_{π^-}) and the nonmesonic decay width (Γ_{nm}) were then derived by combining the results of the present lifetime measurement and the previous data of the π^0 mesonic decay branching ratios. The Γ_n/Γ_p ratios were evaluated by a direct comparison of the observed proton energy spectra with calculated ones as described in the next section.

The (π^+, K^+) reaction has several advantages in the measurement of the weak decay of heavy Λ hypernuclei. Conversely, the (K^-, π^-) reaction, whose momentum transfer is very small, dominantly excites substitutional states and poorly populates the bound region of a Λ hypernucleus [19]. On the contrary, the (π^+, K^+) reaction, whose momentum transfer is about 400 MeV/c, is suitable to excite deeply bound states of a Λ hyperon. Another advantage of the (π^+, K^+) reaction over the (K^-, π^-) reaction is that the pion beams are relatively clean compared with kaon beams, which are subject to a large contamination of pions originated in the in-flight decay. It is crucial for a precise measurement of the branching ratios for heavier Λ hypernuclei such as $^{28}_{\Lambda}$Si to obtain inclusive spectra in which each peak is clearly separated with high statistics and less background contamination.

The present experiment was carried out at the K6 beam line [20] of the KEK 12-GeV Proton Synchrotron (PS), which is depicted in Fig. 1. Primary proton beams were extracted for 1.4–1.8 s in each 4.0 s period. The central momentum of pion beams was set to 1.06 GeV/c, where the production cross section of the elementary (π^+, K^+) reaction becomes maximum [21]. The typical beam intensity at the target was adjusted to $3.6 \times 10^6\,\pi^+$ per 1.8 s for 2.0×10^{12} primary protons to maintain the stability of the total detection efficiency of the tracking chambers on the beam line. The accumulated numbers of incident pions used in the present analysis are listed in Table I.

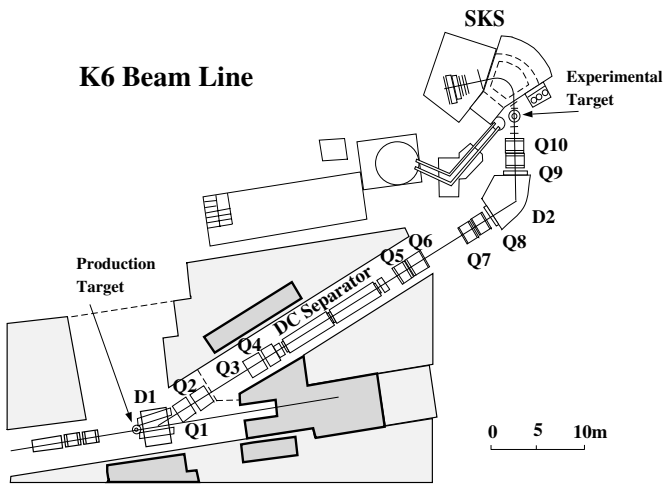

FIG. 1. Schematic view of the KEK-PS K6 beam line and SKS.

Plates of graphite (^{nat}C), natural silicon (^{nat}Si), and iron (^{nat}Fe) were used as the experimental targets. These targets were tilted up by 10–15 degrees from the beam direction to maximize the thickness in the beam direction (6–10 g/cm^2) and minimize the threshold energy of the charged decay particles. Detailed specifications of the experimental targets can be found in Ref. [17].

The momenta of the scattered particles were analyzed by the Superconducting Kaon Spectrometer (SKS). SKS has specifications particularly suitable for coincidence experiments of hypernuclei, such as a large solid angle (100 msr) and short flight length ($\sim$5 m), as well as a good momentum resolution (FWHM $\sim 0.1\%$ at 720 MeV/c) [22]. Kaon events were selected in the mass spectrum of scattered particles, which were reconstructed by their time-of-flight and momentum. The mass of Λ hypernuclei was calculated for selected (π^+, K^+) events through the momentum vectors of incident pions and scattered kaons with corrections of the energy loss in the beam counters and the experimental target. The correction of the horizontal scattering angle measured by SKS was applied to the momenta of outgoing kaons. In addition, constant offsets were applied to the present hypernuclear mass spectra so as to adjust the measured ground states to the ones measured by the previous studies [23–25]. The constant offsets applied for the spectra with the ^{12}C(π^+, K^+),^{28}Si(π^+, K^+), and Fe(π^+, K^+) reactions were 0.62, 3.51, and 2.0 MeV, respectively.

Charged particles emitted in the weak decay of Λ hypernuclei were detected by the decay counter systems located above and below the experimental target, as shown in Fig. 2. Each system was composed of timing scintillation counters (T1 and T2), multiwire drift chambers (PDCU and D), and range counters (RangeU and D). The plastic scintillation counters (T1 and T2) were designed to realize good time resolution ($\sigma \sim 40$ ps) even under the high rate of 10^6 particle/s [26]. The T1 counters installed on the beam line gave the time of hypernuclear production, and the T2 counters located above and below the target measured time information and deposited energy (ΔE) of the decay particles. A detailed description of the fast timing measurement in the present experiment can be found in Ref. [17].

The PDC is a multiwire drift chamber having two plane pairs parallel and one plane-pair perpendicular to the beam direction. The distance between the sensitive wires in each plane was 8 mm, and the elements of each plane pair were displaced relative to the other by a half of the wire spacing to solve the left/right ambiguity. The typical spatial resolution of the PDC was $\sigma \simeq 300\,\mu$m. Tracks of the decay particles were reconstructed by fitting the hit positions on the PDC and the reaction vertex on the target plane.

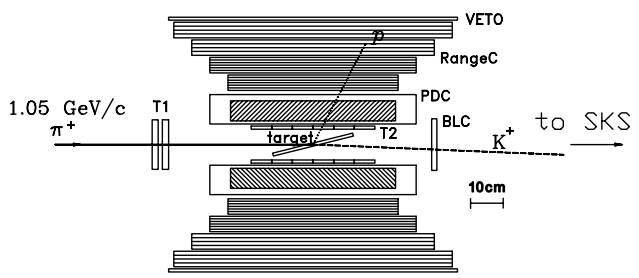

FIG. 2. Schematic view of the decay counter system.

The range counter is composed of twenty plastic scintillators, of which 12 slabs were of 4 mm thickness and 8 slabs were of 6 mm thickness, respectively. The region of kinetic energy measured by the range counter system was from 30 MeV to 150 MeV for protons and from 12 MeV to 70 MeV for pions, respectively. The total kinetic energy deposited in the range counters ($E_{\rm tot}$) was also evaluated by summing up all ADC data after adjusting the pulse height gain of each segment.

Pions and protons were identified with the functions (PID1 and PID2) given by the measured ΔE, range, and $E_{\rm tot}$. These functions were defined as follows:

$$X = \ln(\text{range}),$$
$$Y = \ln(dE/dx),$$
$$Z = \ln(E_{\rm tot}),$$
$$\text{PID1} = Y - P_2(X), \quad (4)$$
$$\text{PID2} = Y - P_2(Z). \quad (5)$$

Here, the mean energy loss (dE/dx) of each decay particle was calculated by the energy deposit (dE) with a correction of the flight length (dx) in the T2 counters. The symbol P_2 denotes a second-order polynomial function, which was used to correct the correlations and make the one-dimensional plot of particle identification functions (PID functions). Protons and pions which passed the criteria of both PID1 and PID2 functions were used in the analysis. Figure 3 shows the PID functions obtained in the $^{12}_{\Lambda}$C ground state region with Gaussian-shape fitting curves. The accepted efficiency of the PID window for pions and protons is $(98.8 \pm 1.2)\%$, and it was included in the estimation of detection efficiency. The proton events in the pion window were evaluated to be less than 1% of pion events, after applying both PID1 and PID2 gates.

The overall solid angle of the two decay counter systems was estimated to be $\Omega_{\rm coin}/4\pi = (27 \pm 1)\%$ for $^{12}_{\Lambda}$C and $_{\Lambda}$Fe, and $\Omega_{\rm coin}/4\pi = (28 \pm 1)\%$ for $^{28}_{\Lambda}$Si by a Monte-Carlo simulation based on GEANT [27]. The error of the solid angle comes from the angle resolution of the drift chambers. The total detection efficiency ($\varepsilon_{\rm coin}$) of each decay counter

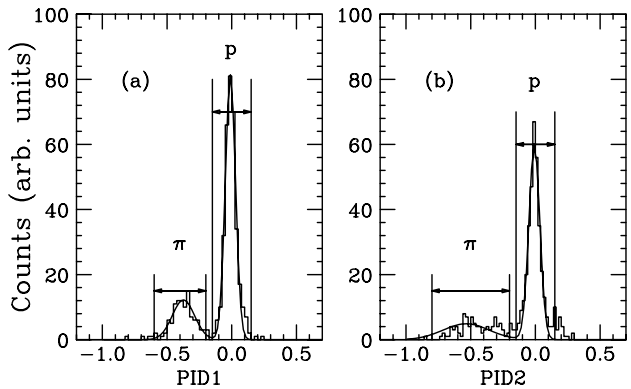

FIG. 3. The particle identification functions in the region of the $^{12}_{\Lambda}$C ground state with fitting curves. (a) PID1 function made from ΔE and range. (b) PID2 function made from ΔE and $E_{\rm tot}$.

system, including the ambiguity of the particle identification, was estimated to be $(84 \pm 2)\%$ for the carbon and iron targets and $(86 \pm 2)\%$ for the silicon target. These efficiencies were obtained by analyzing the calibration data of the (π^+, pp') and $(\pi^+, p\pi)$ reactions, which were taken simultaneously with the (π^+, K^+) trigger data.

The stability of the detection efficiency during the experiment was studied by monitoring the detection efficiency in each data-taking run, which usually took about 2 h. The errors in the detection efficiency are dominantly due to statistics of the calibration data. These errors in the evaluation of the solid angle and the detection efficiency are included in the systematic errors of the branching ratios.

III. ANALYSIS AND RESULTS

A. Hypernuclear mass spectra

Figures 4–6 illustrate the measured hypernuclear mass spectra. The horizontal axis is the mass difference between a produced Λ hypernucleus and a target nucleus $(M_{HY} - M_A)$. A scale in the binding energy of the Λ hyperon (B_Λ) is also given in the same figure. The top spectrum (a) in each figure is the inclusive spectrum of the (π^+, K^+) reaction. The middle and bottom spectra, (b) and (c), are the coincidence spectra with protons $(E_p > 40$ MeV) and charged pions $(E_\pi > 12.5$ MeV), respectively.

In Figs. 4(a) and 5(a), the two dominant peaks, denoted as s_Λ and p_Λ at $B_\Lambda = 10.8$ and -0.1 MeV for $^{12}_{\Lambda}$C and $B_\Lambda = 16.6$ and 7.1 MeV for $^{28}_{\Lambda}$Si, were interpreted as the neutron-hole Λ-particle configurations of $[0p^{-1}_{3/2}, s_\Lambda]$ and $[0p^{-1}_{3/2}, p_\Lambda]$ for $^{12}_{\Lambda}$C and those of $[0d^{-1}_{5/2}, s_\Lambda]$ and $[0d^{-1}_{5/2}, p_\Lambda]$ for $^{28}_{\Lambda}$Si, respectively. The quasifree Λ production process rises from its threshold $(B_\Lambda = 0$ MeV). Compared to the previous hypernuclear weak decay experiments carried out at BNL [5] and KEK [7], the background level in Fig. 4(a) is greatly improved, and each peak can be clearly identified.

The peak assignments and interpretations of $^{12}_{\Lambda}$C and $^{28}_{\Lambda}$Si hypernuclei are taken from the previous spectroscopic study of light-to-heavy Λ hypernuclei with SKS [24] and theoretical investigations [28]. Because the hypernuclear spectra of $^{12}_{\Lambda}$C with a resolution of 2 MeV in (FWHM) revealed that the subpeaks between the predominant ones have about 10% strength to the dominant ones, these subpeaks were taken into account in the present peak fitting.

The fitting functions applied for the inclusive and coincidence spectra on ^{12}C(π^+, K^+) and ^{28}Si(π^+, K^+) reactions are as follows:

$$f(x) = \sum_{i=1}^{n} g_i(x - x_i) + QF(x) + \text{const.} \quad (n = 4{,}5 \text{ for } ^{12}_{\Lambda}\text{C and } ^{28}_{\Lambda}\text{Si}) \tag{6}$$

$$g_i(x) = \frac{A_i}{\sqrt{2\pi}\sigma_i} \exp\left(-\frac{x^2}{2\sigma_i^2}\right) \quad \left[\text{for the } i\text{-th peak}, \quad \sigma_i = \sqrt{\sigma^2 + \left(\sigma_i^{\text{old}}\right)^2}\,\right] \tag{7}$$

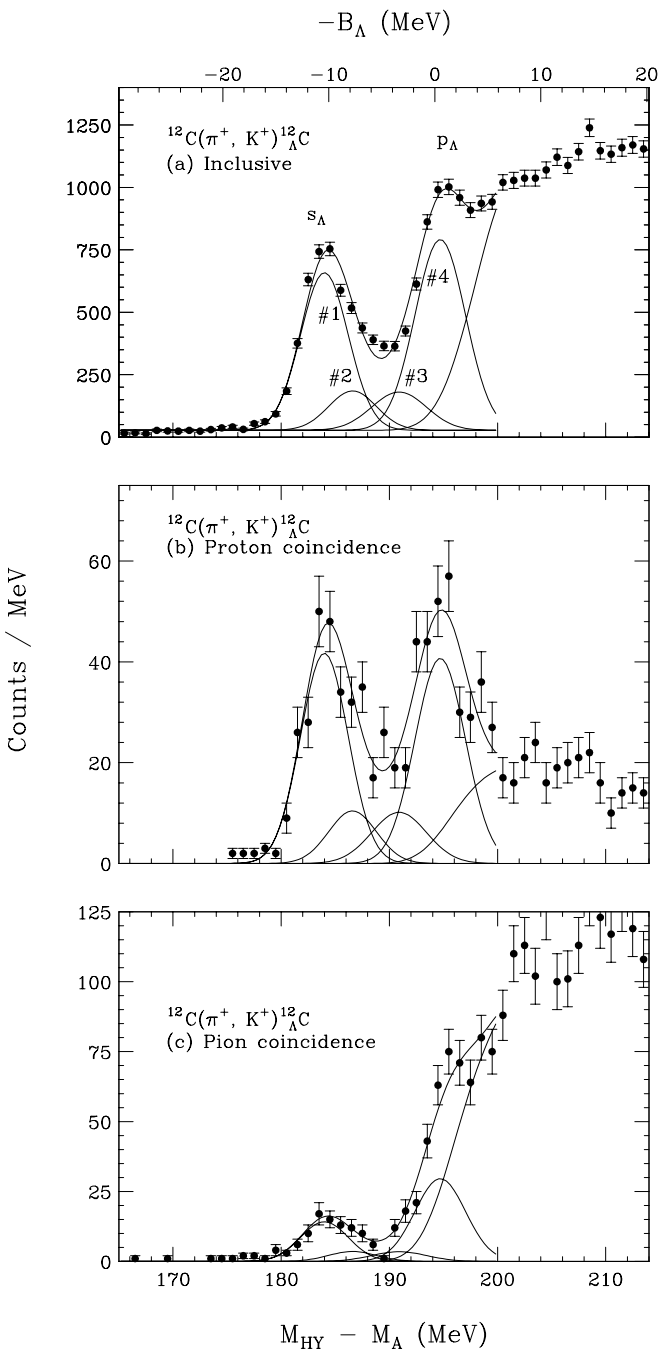

FIG. 4. Hypernuclear mass spectra by the ^{12}C(π^+, K^+) reaction; (a) inclusive, (b) with coincident protons $(E_p > 40$ MeV), and (c) with coincident pions $(E_\pi > 12.5$ MeV).

$$QF(x) = \frac{1}{\sqrt{2\pi}\sigma_1} \int R(x - x_{\text{th}} + q) \exp\left(-\frac{q^2}{2\sigma_1^2}\right) dq \tag{8}$$

$$R(t) = \begin{cases} a\sqrt{t} + bt + ct^2 + dt^3 & \text{for } t > 0 \\ 0 & \text{otherwise} \end{cases}, \tag{9}$$

where the peak position (x_i), relative intensity to the ground state (A_i/A_1), and peak width (σ_i^{old}) of each Gaussian-like function were taken from the previous experimental

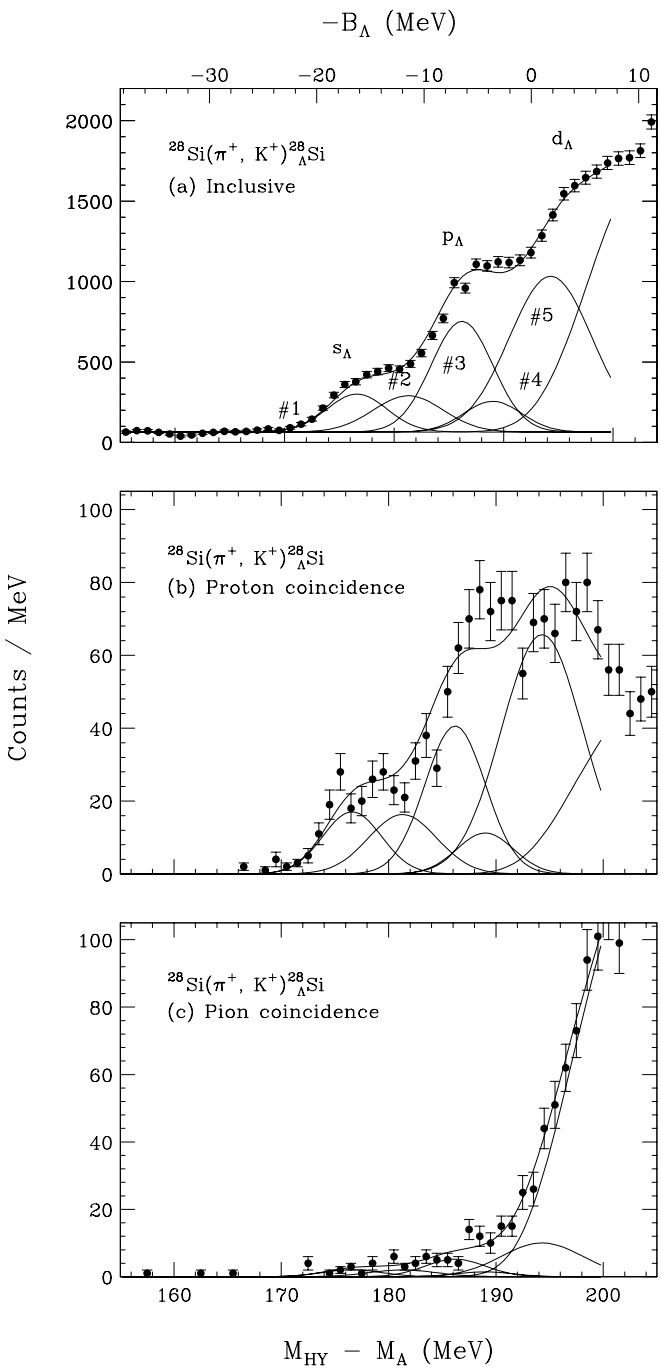

FIG. 5. Hypernuclear mass spectra by the ^{28}Si(π^+, K^+) reaction; (a) inclusive, (b) with coincident protons ($E_p > 40$ MeV), and (c) with coincident pions ($E_\pi > 12.5$ MeV).

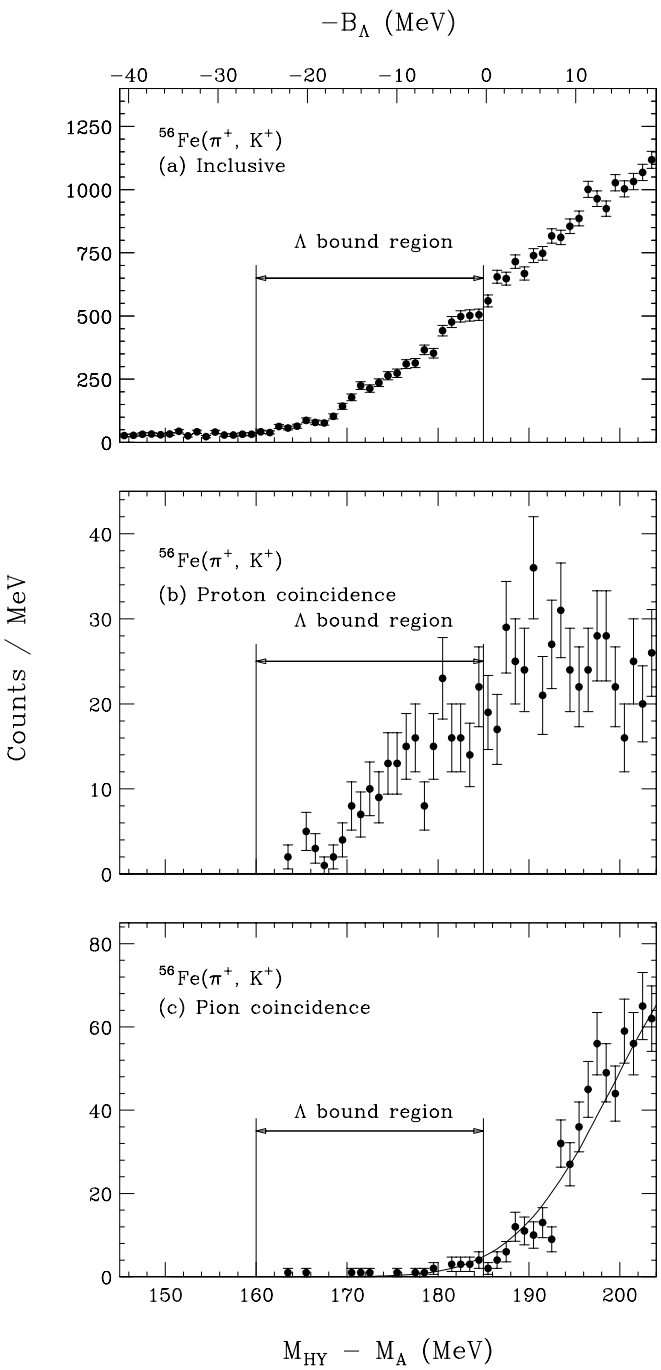

FIG. 6. Hypernuclear mass spectra by the Fe(π^+, K^+) reaction; (a) inclusive, (b) with coincident protons ($E_p > 40$ MeV), and (c) with coincident pions ($E_\pi > 12.5$ MeV).

results [24]. The parameter σ was adjusted at first by fitting the ground state for $^{12}_{\Lambda}$C and $^{28}_{\Lambda}$Si in the proton coincidence spectra, representing the effect on the energy resolution because the present targets are much thicker than those in the previous singles experiment. The function for the quasifree continuum [$R(t)$] was assumed to be a sum of the squared-root type function and third-order polynomial function convoluted with the width of the ground state (σ_1) as shown in Eq. (9). A constant background was also assumed. The measured energy resolutions of the ground state in the ^{12}C(π^+, K^+) and ^{28}Si(π^+, K^+) spectra were 4.8 and 6.3 MeV in FWHM, respectively. In the fitting of the ^{12}C(π^+, K^+) and ^{28}Si(π^+, K^+) inclusive spectra, the free parameters were the yield of the prominent peak (A_1) and the shape of quasifree continuum (a–d).

In Figs. 4(b) and 4(c), the peak positions of two subpeaks (2 and 3) are lower than the energy threshold of proton emission and these states supposedly decay to the ground state

by emitting γ rays. Because the lifetimes of these states are supposed to be on the order of 1 ps, which is much shorter than those of the typical hypernuclear weak decay ($\tau \sim 200$–300 ps), the subpeak events can be regarded as the ones by the weak decay from the $^{12}_{\Lambda}$C ground state. Conversely, it is known from the old emulsion experiments that the p_Λ state of $^{12}_{\Lambda}$C emits a proton and sequentially produces $^{11}_{\Lambda}$B hypernucleus, which then deexcites to the ground state and eventually decays due to the weak interaction [29,30]. Therefore, events in the p_Λ state can be thought as those due to the weak decay of $^{11}_{\Lambda}$B.

It is confirmed by the previous experimental study [31,32] that quasifree Λ hyperons can make Λ hypernuclei in the target. Those Λ hypernuclei eventually emit protons by the nonmesonic decay. Therefore, the tagged protons in the quasifree region can be regarded as the ones associated with the nonmesonic decay of Λ hypernuclei, not as misidentified pions.

In the fitting of Figs. 4(b) and 4(c), the yield of $p_\Lambda(A_4)$ was also treated as free parameters. For peaks 2 and 3, their relative intensity and position to the peak 1 in the inclusive spectrum were kept constant. The free parameters were the yields of peaks 1 and 4, and the shape of quasifree continuum. In Figs. 5(b) and 5(c), the p_Λ states (3 and 4) located above the proton emission threshold can be regarded as those of the weak decay of $^{27}_{\Lambda}$Al after emitting a proton. Therefore, the yields of the dominant peak (1, 3, and 5) were treated as free parameters, whereas the relative peak intensity of each subpeak (2 and 4) to the dominant one (1 and 3) was fixed to be constant.

In the Fe(π^+, K^+) spectrum, events gated in the region of a Λ hyperon bound to the ^{55}Fe nucleus were used in the analysis since each hypernuclear state could not be separated. Considering the proton emission threshold of the excited states of $^{56}_{\Lambda}$Fe, a series of Λ hypernuclei ($^{56}_{\Lambda}$Fe, $^{55}_{\Lambda}$Mn, and $^{55}_{\Lambda}$Fe) can be included in the gated region. The symbol $_{\Lambda}$Fe represents those Λ hypernuclei whose mass numbers are close to $A \sim 56$.

The yields and statistical errors of $^{12}_{\Lambda}$C,$^{11}_{\Lambda}$ B,$^{28}_{\Lambda}$Si, and $^{27}_{\Lambda}$Al are summarized in Table I. The systematic errors due to the choice of functional shapes for the quasifree region were examined with square-root and polynomial functions. No significant difference was found on the results of the s_Λ state of $^{12}_{\Lambda}$C and $^{28}_{\Lambda}$Si. However, significant systematic changes of about 20% for $^{12}_{\Lambda}$C and 50% for $^{28}_{\Lambda}$Si were found in the results on the p_Λ states. Such variations were included in the systematic errors of the π^- branching ratios of $^{11}_{\Lambda}$B and $^{27}_{\Lambda}$Al.

TABLE I. The number of incident pions used in the present analysis and the estimated yields of each hypernuclear state.

	$N_{\pi^+}(\times 10^9)$	Y_{HY}	Y_p	Y_{π^-}
$^{12}_{\Lambda}$C	314	4132 ± 70	273 ± 17	93 ± 10
$^{11}_{\Lambda}$B		4016 ± 92	$213 \pm 20 \pm 18$	$155 \pm 24 \pm 32$
$^{28}_{\Lambda}$Si	620	2631 ± 74	190 ± 15	23 ± 5
$^{27}_{\Lambda}$Al		3693 ± 83	218 ± 20	$28 \pm 7 \pm 13$
$_{\Lambda}$Fe	919	3981 ± 96	222 ± 15	23 ± 5

TABLE II. The π^- mesonic decay branching ratios (b_{π^-}) obtained in the present analysis and the mesonic decay branching ratios ($b_m = b_{\pi^-} + b_{\pi^0}$). The quoted errors are statistical and systematic, respectively.

	b_{π^-} ($\times 10^{-2}$)	b_{π^0} ($\times 10^{-2}$)	b_m ($\times 10^{-2}$)
$^{12}_{\Lambda}$C	$9.9 \pm 1.1 \pm 0.4$	$17.4 \pm 5.7 \pm 0.8$ [6]	$27.3 \pm 1.1 \pm 5.8$
$^{11}_{\Lambda}$B	$17.0 \pm 2.7 \pm 3.6$	$14.0 \pm 3.9 \pm 2.5$ [6]	$31.0 \pm 2.7 \pm 5.9$
$^{28}_{\Lambda}$Si	$3.6 \pm 0.8 \pm 0.2$	8.3 ± 8.3[a]	$11.9 \pm 0.8 \pm 8.3$[a]
$^{27}_{\Lambda}$Al	$3.2 \pm 0.8 \pm 1.5$	2.0 ± 2.0[a]	$5.2 \pm 0.8 \pm 2.5$[a]
$_{\Lambda}$Fe	<1.2 (90% CL)		1.5 ± 1.5 [9]

[a]The ratios of $\Gamma_{\pi^0}/\Gamma_{\pi^-}$ were assumed to be 2.30 for $^{28}_{\Lambda}$Si and 0.65 for $^{27}_{\Lambda}$Al with 100% errors, according to the theoretical calculations by Motoba *et al*. [9].

For $_{\Lambda}$Fe hypernuclei, the number of events in the gated window was used to estimate the yields. The expected number of true pion events in the bound region of a Λ particle was evaluated to be less than 12.4 at the 90% confidence level (CL) by fitting the quasifree region in Fig. 6(c). Only an upper limit of the π^- mesonic decay branching ratio was obtained for $_{\Lambda}$Fe.

B. Branching ratios of the mesonic and nonmesonic decay

The branching ratios of the mesonic decay and the nonmesonic decay can be expressed by the experimental observables as follows:

$$b_{\pi^-} = \frac{\Gamma_{\pi^-}}{\Gamma_{\rm tot}} \tag{10}$$

$$= \frac{Y_{\pi^-}}{Y_{HY}} (\varepsilon_{\rm coin}\Omega_{\rm coin})^{-1}, \tag{11}$$

$$b_m = b_{\pi^-} + b_{\pi^0}, \tag{12}$$

$$b_{nm} = 1 - b_m, \tag{13}$$

where the symbols of Y_{HY} and Y_{π^-} represent the yields of each Λ hypernucleus and associated decay pions, as described in the previous section. The symbol $\varepsilon_{\rm coin}\Omega_{\rm coin}$ denotes a product of the detection efficiency and the solid angle of the decay counter system, which was discussed in Sec. II. Table II shows the results of the π^- mesonic decay branching ratios (b_{π^-}) of $^{12}_{\Lambda}$C and $^{28}_{\Lambda}$Si hypernuclei. An upper limit of the branching ratio of the π^- mesonic decay on $_{\Lambda}$Fe was evaluated at the 90% CL.

Figure 7 shows the energy distribution of pions emitted by $^{12}_{\Lambda}$C. The pion energy threshold was set at 12.5 MeV. It was found that more than 99% of the pion events in the energy spectrum were accepted based on a simulation taking into account the energy level distributions of the daughter nucleus, ^{12}N, calculated in Ref. [8].

Branching ratios of the nonmesonic weak decay were derived incorporating those of charged and neutral mesonic weak decay. As for $^{12}_{\Lambda}$C and $^{11}_{\Lambda}$B, the π^0 mesonic decay branching ratios (b_{π^0}) were taken from the previous experimental data [6].

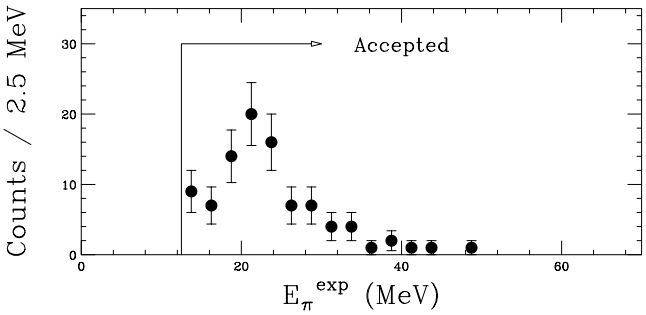

FIG. 7. The pion energy spectrum of ${}^{12}_{\Lambda}$C. The vertical axis is normalized to the total counts in the experimental data.

The errors of the π^0 branching ratios were treated as the systematic ones in the present result. As for ${}^{28}_{\Lambda}$Si and ${}^{27}_{\Lambda}$Al, the ratios of the π^0 to π^- decay width ($\Gamma_{\pi^0}/\Gamma_{\pi^-}$) were assumed to be 2.30 for ${}^{28}_{\Lambda}$Si and 0.65 for ${}^{27}_{\Lambda}$Al, respectively, according to the theoretical calculations [9]. The calculated ratios of $\Gamma_{\pi^0}/\Gamma_{\pi^-}$ were adopted to the present results. The errors of the adopted π^0 branching ratios for ${}^{28}_{\Lambda}$Si and ${}^{27}_{\Lambda}$Al were assumed to be 100%. The mesonic decay branching ratio of ${}_{\Lambda}$Fe was also taken from the theoretical calculation to be 0.015 [9]. The uncertainty of b_m was assumed to be 100%.

C. Proton energy spectra and Γ_n/Γ_p ratios

Figure 8 shows the proton energy spectra measured in the present experiment. The number of protons measured by the decay counters is plotted as a function of the proton energy measured by the range counter ($E_p^{\rm exp}$). It is emphasized that $E_p^{\rm exp}$ denotes the kinetic energy of the decay protons at the range counter, but not the one at the weak decay vertex because the decay protons generated at the reaction vertex undergo energy loss and struggling processes in the experimental target and the T2 counter. The proton energy spectrum is normalized by the number of hypernuclear weak decays as follows:

$$R_p^{\rm exp}\left(E_p^{\rm exp}\right) = \frac{Y_{\rm coin}\left(E_p^{\rm exp}\right)}{Y_{\rm inclusive}}, \tag{14}$$

where $Y_{\rm inclusive}$ represents the number of events in the inclusive hypernuclear-mass spectrum and $Y_{\rm coin}(E_p^{\rm exp})$ is the one in the corresponding proton-coincidence spectrum. The error bars plotted in the spectra are statistical ones only. The events above 40 MeV are analyzed to avoid the uncertainty of the detection limit near 30 MeV.

In accord with Ref. [33], the initial proton energy spectra at the vertex of the nonmesonic weak decay were calculated with the pion-exchange potential and local density approximation in finite nuclei, assuming various Γ_n/Γ_p ratios on ${}^{12}_{\Lambda}$C,${}^{28}_{\Lambda}$Si, and ${}_{\Lambda}$Fe hypernuclei. After the nonmesonic decay, the outgoing nucleons propagate through the nucleus colliding with other nucleons, the so-called intranuclear cascade process (INC). Authors of Refs. [33,34] calculated the proton energy spectra emitted from nuclei with help of the INC code [35].

In Refs. [33,34], the proton energy spectra generated by the proton- and neutron-induced nonmesonic decay were summed incoherently for a given Γ_n/Γ_p ratio. Explicitly, the number of protons emitted in a nonmesonic weak decay can be expressed

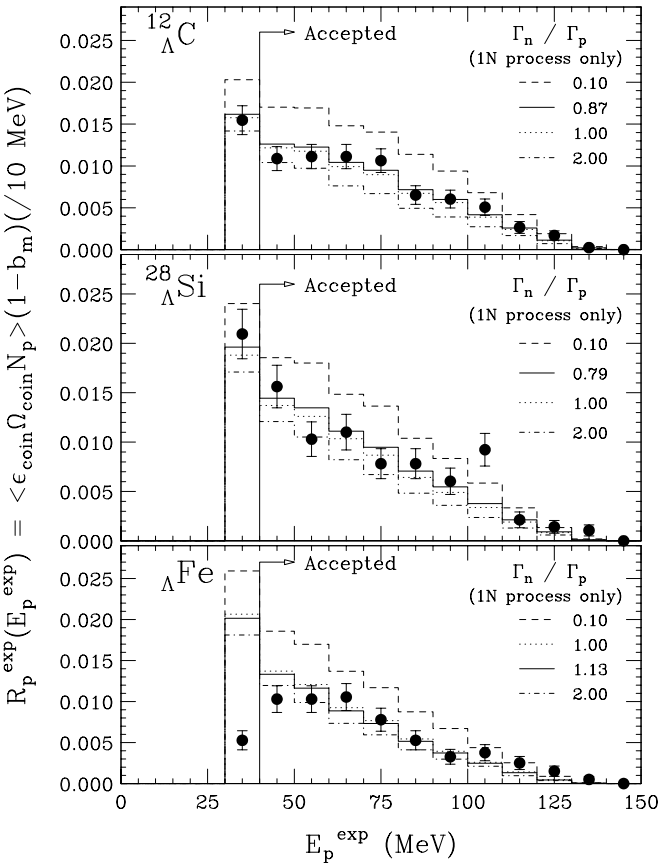

FIG. 8. Comparison of the simulated energy spectra with the experimental data. The horizontal axis is the observed energy by the decay counter. The vertical axis is normalized by the number of hypernuclear weak decays.

as a function of proton energy (E_p) and Γ_n/Γ_p ratio as follows:

$$N_p(E_p;\Gamma_n/\Gamma_p) = \begin{cases} a_n N_p^{\rm ini}(E_p;\Gamma_n) + a_p N_p^{\rm ini}(E_p;\Gamma_p) & \\ \quad \times (a_n + a_p = 1) & \text{for } 1N \text{ process only} \\ a_n N_p^{\rm ini}(E_p;\Gamma_n) + a_p N_p^{\rm ini}(E_p;\Gamma_p) + a_{2N} N_p^{\rm ini}(E_p;\Gamma_{2N}) & \\ \quad \times (a_n + a_p + a_{2N} = 1) & \text{for } 1N + 2N \text{ process,} \end{cases} \tag{15}$$

where a_n, a_p, and a_{2N} are the fractions of neutron- and proton-induced nonmesonic decay ($\Lambda \to NN$) and the two-nucleon induced decay ($\Lambda NN \to NNN$), respectively. $N_p^{\rm ini}(E_p;\Gamma_n)$ and $N_p^{\rm ini}(E_p;\Gamma_p)$ are the numbers of protons originated in the neutron- and proton-induced process, the so-called $1N$ process, and $N_p^{\rm ini}(E_p;\Gamma_{2N})$ is that originated in the two-nucleon induced decay, the so-called $2N$ process, respectively. The number of protons in the above equation is normalized to be the one per nonmesonic weak decay of a Λ hypernucleus.

The proton energy spectra measured by the decay counters were calculated by the GEANT simulation code described in the previous section. In the Monte Carlo simulation, energetic protons emitted from the target nucleus with the energy distributions of protons [$N_p(E_p;\Gamma_n/\Gamma_p)$] were transported through the target material and the decay counters. The geometrical acceptance, the energy loss, and its straggling

TABLE III. Nonmesonic decay widths and Γ_n/Γ_p ratios in the present experiment. All the decay widths are listed in units of the total decay width of a Λ hyperon in free space (Γ_Λ).

	$\Gamma_{nm}/\Gamma_\Lambda$	Γ_n/Γ_p		
		"$1N$ only"	"$1N$ and $2N$"	Refs.
Experiment				
$^{12}_{\Lambda}$C	$0.828 \pm 0.056 \pm 0.066$	$0.87 \pm 0.09 \pm 0.21$	$0.60^{+0.11+0.23}_{-0.09-0.21}$ ($\Gamma_{1N}=0.80$, $\Gamma_{2N}=0.28$) [33]	Present[a]
	$0.89 \pm 0.15 \pm 0.03$	$1.87 \pm 0.59^{+0.32}_{-1.00}$		[7]
	1.14 ± 0.20	$1.33^{+1.12}_{-0.81}$		[5]
$^{11}_{\Lambda}$B	$0.861 \pm 0.063 \pm 0.073$			Present
	$0.95 \pm 0.13 \pm 0.04$	$2.16 \pm 0.58^{-0.45}_{-0.95}$		[7]
		$1.04^{+0.59}_{-0.48}$		[5]
$^{28}_{\Lambda}$Si	$1.125 \pm 0.067 \pm 0.106$	$0.79^{+0.13+0.25}_{-0.11-0.24}$	$0.53^{+0.13+0.25}_{-0.12-0.24}$ ($\Gamma_{1N}=0.94$, $\Gamma_{2N}=0.28$) [33]	Present[a]
$^{27}_{\Lambda}$Al	$1.230 \pm 0.062 \pm 0.032$			Present
$_{\Lambda}$Fe	1.21 ± 0.08	$1.13^{+0.18+0.23}_{-0.15-0.22}$	$0.87^{+0.18+0.23}_{-0.15-0.21}$ ($\Gamma_{1N}=1.02$, $\Gamma_{2N}=0.27$) [33]	Present[a]
Theory				
$^{12}_{\Lambda}$C	1.060	0.368		[41]
	0.82			[42]
	0.726	0.288		NSC97a [45]
	0.554	0.341		NSC97f [45]
$^{28}_{\Lambda}$Si	1.556	0.402		[41]
	1.02			[42]
$^{56}_{\Lambda}$Fe	1.679	0.455		[41]
	1.12			[42]
$p+^{209}$Bi	$1.82 \pm 0.09 \pm 0.29$[b]			[40]
$p+^{238}$U	1.10 ± 0.28[b]			[39]
$A=\infty$	2.456	0.716		$\pi + K + DQ$ [44]

[a]The uncertainty of theoretical calculations in the proton energy spectra is not included in the systematic errors.

[b]The results of lifetime measurements were converted to the nonmesonic decay widths, assuming that no mesonic decay occurs in heavy Λ hypernuclei.

in the target and decay counters together with the energy threshold of 40 MeV were automatically taken into account. The notation of $< \Omega_{\rm coin} N_p(E_p; \Gamma_n/\Gamma_p) >$ is introduced to represent the proton energy spectra obtained by the GEANT simulation code.

The simulated proton energy spectrum $[R_p^{\rm cal}(E_p^{\rm exp})]$ to be compared with the experimental data $[R_p^{\rm exp}(E_p^{\rm exp})]$ was obtained as follows:

$$R_p^{\rm cal}\left(E_p^{\rm exp}\right) = < \Omega_{\rm coin} N_p(E_p; \Gamma_n/\Gamma_p) > \varepsilon_{\rm coin} b_{nm}, \qquad (16)$$

where $\varepsilon_{\rm coin}$, $\Omega_{\rm coin}$, and b_{nm} represent the detection efficiency, the solid-angle acceptance of the decay counters, and the branching ratio of the nonmesonic decay described in the previous section, respectively.

The Γ_n/Γ_p ratios of $^{12}_{\Lambda}$C,$^{28}_{\Lambda}$Si, and $_{\Lambda}$Fe were obtained by fitting the experimental data with the simulated spectra, changing the Γ_n/Γ_p ratio as a free parameter. The results in both cases of the $1N$-only and $1N$ and $2N$ processes are listed in Table III. The simulated proton energy spectra in the case of $\Gamma_n/\Gamma_p = 0.1$, 1.0, and 2.0 are overlaid on the experimental data in Fig. 8. It is shown that the proton yield is much smaller than the calculated one assuming $\Gamma_n/\Gamma_p = 0.1$, which seems to exclude very small values of Γ_n/Γ_p.

Recently, an Erratum of Ref. [33] was published, giving the new proton energy spectra [36]. Because much stronger final state interaction in the INC process was applied in the updated spectra than that in the original article, the shape of the spectra was greatly shifted toward the lower energy side. The present results of the Γ_n/Γ_p ratios listed in Table III are updated from the ones published in our previous report [18] by applying the new proton energy spectra given by the authors of Ref. [36] to the experimental data. It should be noted that the experimental proton energy spectra published in Ref. [18] themselves do not change at all in the present report. Because the experimental data of proton energy spectra noted in Eq. (14) contains only experimental observables, they are free from theoretical assumptions. As a result, the Γ_n/Γ_p ratios of $^{12}_{\Lambda}$C and $^{28}_{\Lambda}$Si became smaller than our previous ones published in Ref. [18].

The statistical error of each Γ_n/Γ_p ratio for $^{12}_{\Lambda}$C,$^{28}_{\Lambda}$Si, and $_{\Lambda}$Fe was evaluated by the conventional least-squares method. In addition, the systematic error was evaluated considering the uncertainty of the nonmesonic decay branching ratio, the detection efficiency of the decay counters, and the solid angle acceptance. The systematic errors of the ratio $R_p^{\rm cal}(E_p^{\rm exp})$ in Eq. (16) were found to be 0.09, 0.10, and 0.05 for $^{12}_{\Lambda}$C,$^{28}_{\Lambda}$Si, and $_{\Lambda}$Fe, respectively. For $_{\Lambda}$Fe, the dependence of the gate position

for the Λ bound state on the Γ_n/Γ_p ratio was also examined. The differences of the obtained Γ_n/Γ_p ratios for 160 MeV $< M_{HY} - M_A <$ 180 MeV and 160 MeV $< M_{HY} - M_A <$ 190 MeV were found to be 13% for the 1*N* process and 15% for the 1*N*+2*N* process. These errors were included in the systematic errors for ${}_{\Lambda}$Fe.

Assuming that the decay widths of the 1*N* and 2*N* process are 0.803 and 0.277 on ${}^{12}_{\Lambda}$C [33,34], the Γ_n/Γ_p ratio on ${}^{12}_{\Lambda}$C is $0.60^{+0.11+0.23}_{-0.09-0.21}$. Recently, Alberico *et al*. evaluated the decay width of the 2*N* process to be 0.16 on ${}^{12}_{\Lambda}$C, based on the propagator method [42,46]. When we take this value, the Γ_n/Γ_p ratio of ${}^{12}_{\Lambda}$C changes from 0.60 to 0.70. Because most of protons emitted by the 2*N* process are not detected by our decay counter systems, the inclusion of the 2*N* process in the fitting gives smaller Γ_n/Γ_p ratios than those in the case of 1*N* process only. The systematic error of the present data listed in Table III was evaluated only by the experimental conditions described above. The uncertainties of the derived Γ_n/Γ_p ratios due to theoretical assumptions and models, such as degree of the 2*N* process contribution and the ambiguity coming from the intranuclear cascade calculations, are not included in the systematic errors quoted in the present results.

IV. DISCUSSION

A. Mesonic decay widths

Table IV and Fig. 9 summarize the present results for the mesonic decay widths together with those obtained by Szymanski *et al*. [5] and Noumi *et al*. [7]. The results of Γ_{π^-} were derived from the obtained branching ratios using the total decay widths measured simultaneously in the present experiment [16,17] by the relation $\Gamma_{\pi^-} = \Gamma_{\rm tot} b_{\pi^-}$. The present π^- decay widths of ${}^{12}_{\Lambda}$C and ${}^{11}_{\Lambda}$B hypernuclei are much more precise than the previous experimental data and allow us a critical comparison with theoretical calculations. Furthermore, finite values of Γ_{π^-} for ${}^{28}_{\Lambda}$Si and ${}^{27}_{\Lambda}$Al were measured for the first time. For ${}_{\Lambda}$Fe, an upper limit of the π^- mesonic decay width was obtained.

TABLE IV. Mesonic decay widths with theoretical calculations. All the decay widths are listed in units of the total decay width of a Λ hyperon in free space (Γ_Λ).

	$\Gamma_{\pi^-}/\Gamma_\Lambda$	Refs.
Experiment		
${}^{12}_{\Lambda}$C	$0.113 \pm 0.014 \pm 0.005$	Present
	$0.14 \pm 0.07 \pm 0.03$	[7]
	$0.052^{+0.063}_{-0.035}$	[5]
${}^{11}_{\Lambda}$B	$0.212 \pm 0.036 \pm 0.045$	Present
	$0.23 \pm 0.06 \pm 0.03$	[7]
${}^{28}_{\Lambda}$Si	$0.046 \pm 0.011 \pm 0.002$	Present
${}^{27}_{\Lambda}$Al	$0.041 \pm 0.010 \pm 0.019$	Present
${}_{\Lambda}$Fe	<0.015(90% CL)	Present
Theory		
${}^{12}_{\Lambda}$C	0.058 (FREE)	[8]
	0.134 (MSU)	[8]
	0.107 (WHIS)	[8]
	0.098 (FULL)	[9]
	0.086 (Nieves)	[10]
${}^{11}_{\Lambda}$B	0.134 (FREE)	[8]
	0.294 (MSU)	[8]
	0.223 (WHIS)	[8]
	0.213 (FULL)	[9]
${}^{28}_{\Lambda}$Si	0.027 (FULL)	[9]
${}^{27}_{\Lambda}$Al	0.065 (FULL)	[9]

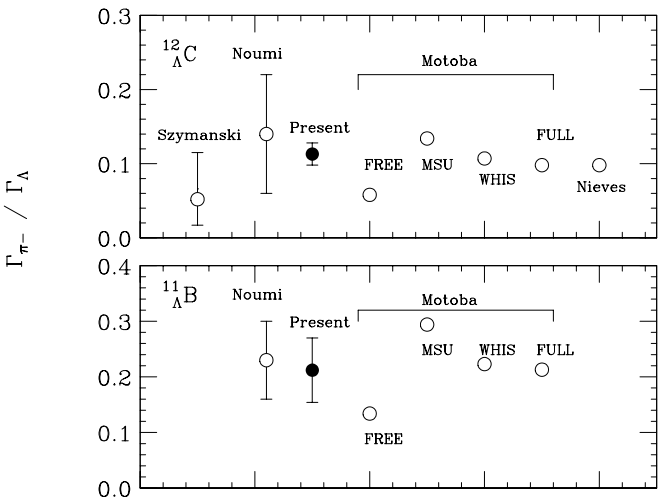

FIG. 9. Comparison of the existing and present data with theoretical calculations by Motoba *et al*. [8,9] and Nieves *et al*. [10]. "FREE" uses a plane wave and only the Coulomb potential for the pion wave function. "MSU" uses an optical potential developed by a group of Michigan State University [37]. "WHIS" uses an optical potential developed by Whisnant [38]. "Nieves" uses a theoretical calculation by Nieves *et al*. "Szym" and "Noumi" are the previous experimental data by Szymanski *et al*. [5] and Noumi *et al*. [7], respectively. The closed circles are the present results.

In Ref. [8], Motoba *et al*. calculated the mesonic decay widths of ${}^{12}_{\Lambda}$C and ${}^{11}_{\Lambda}$B with the pion-nucleus optical potentials given by a group at Michigan State University (MSU) [37] and Whisnant [38] that have a strong and weak imaginary part, respectively. Another potential was introduced to resolve the singularity in the pion wave function (FULL) [9]. The calculated results are compared to the calculations with the plane wave, including the Coulomb distortion (FREE). In addition, Nieves *et al*. have developed an optical potential, which was derived from a purely theoretical calculation, and can reproduce the experimental data of pionic atoms and π-nucleus scattering data [10]. They applied their optical potential to the mesonic decay of Λ hypernuclei incorporating the nuclear shell model wave functions. A similar comparison of the experimental results for the π^- mesonic decay of ${}^{28}_{\Lambda}$Si and ${}^{27}_{\Lambda}$Al with the theoretical results is also shown in Table IV only for the case of "FULL."

It can be said that theoretical calculations taking into account the distortion effects of the pion wave function and nuclear wave functions agree well with the present experimental results. In particular, the result on ${}^{12}_{\Lambda}$C, whose experimental error has been drastically improved, is consistent with an increase of Γ_{π^-} due to the distortion of the pion wave function by the pion-nucleus optical potentials.

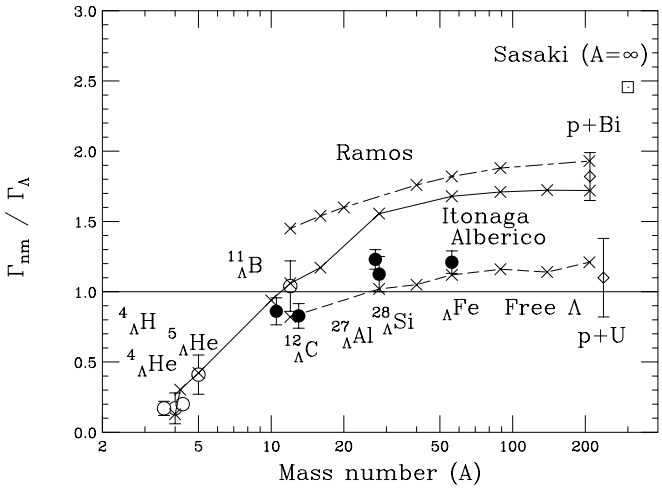

FIG. 10. Total nonmesonic decay widths of Λ hypernuclei. The open circles are previous experimental data in which the hypernuclear production was explicitly identified. The open diamonds are experimental data by the $p + \mathrm{Bi}$ and $p + \mathrm{U}$ reactions with the recoil shadow method in which the production of strangeness was not explicitly identified. The solid circles are the present results. The solid line is a calculation by Itonaga *et al*. [41]. The dash-dotted line is a calculation by Ramos *et al*. [43]. The dashed line is a calculation by Alberico *et al*. [42] (Γ_{1N} only). The open square shows a result with the direct quark exchange model in nuclear medium by Sasaki *et al*. [44].

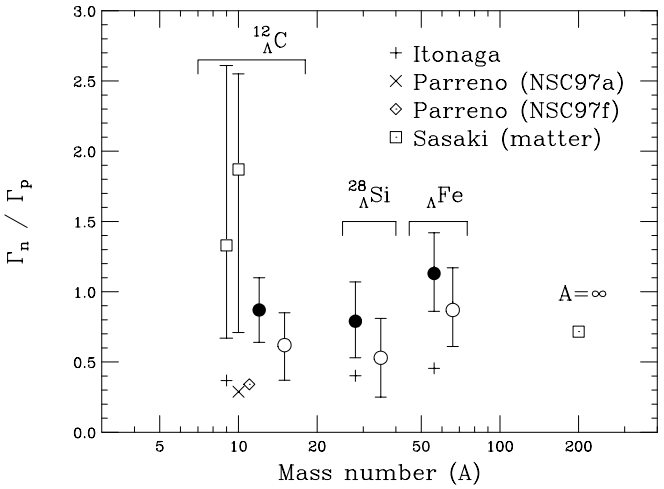

FIG. 11. The Γ_n/Γ_p ratios of Λ hypernuclei. The closed and open circles are the results of the present experiment, assuming the "1*N* only" and "1*N* and 2*N*" processes, respectively. The open squares are previous experimental data by Szymanski *et al*. [5] and Noumi *et al*. [7]. Theoretical calculations by Itonaga [41], Parreno [45], and Sasaki [44] are plotted.

B. Nonmesonic decay widths and Γ_n/Γ_p ratios

Table III summarizes experimental results of nonmesonic decay width and Γ_n/Γ_p ratios along with theoretical ones. Figure 10 shows the mass-number dependence of the nonmesonic weak decay widths derived by the present and previous experiments. There are experimental data of lifetime measurement for very heavy hypernuclei in the mass region of $A \sim 200$ with recoil shadow method on $p + \mathrm{Bi}$ and $p + \mathrm{U}$ reactions at COSY, although the strangeness production was not explicitly identified [39,40]. The plotted data around $A \sim 200$ in Fig. 10 were the ones converted from the results of lifetime measurements, assuming that no mesonic decay occurs in heavy Λ hypernuclei. Theoretical calculations of the nonmesonic decay widths by Itonaga *et al*. [41], Ramos *et al*. [43], Alberico *et al*. [42], and Sasaki *et al*. [44] are also illustrated in the figure.

The calculation by Ramos *et al*. [43], on which present derivation of Γ_n/Γ_p ratios rely, was based on one-pion exchange potential in which the vertex renormalization effect in the nuclear medium and the local density approximation are taken into account. Their results of the nonmesonic decay widths are much larger than the experimental results and do not seem to saturate around $A = 56$. Recently, Alberico *et al*. [42] updated Ramos's calculation and obtained results closer to the present data by adjusting the Landau-Migdal parameter, which controls the short-range part of the pion potential.

The present data substantially improved the knowledge of the Γ_n/Γ_p ratios for $^{12}_{\Lambda}$C and $^{11}_{\Lambda}$B as shown in Fig. 11. Although all available experimental data agree with the present ones within 1 sigma level, the present Γ_n/Γ_p's are in the region around 0.5–1.0, whereas the previous ones were significantly larger than unity.

The direct quark current exchange model (DQ) was applied to explain the very short-range part of the nonmesonic decay in light Λ hypernuclei and nuclear matter [15,44], incorporating it with the contribution of π and K meson exchanges. Parreno *et al*. carried out a systematic study about various combinations of meson exchange potentials, such as π, K, η, ρ, and ω mesons [45], which contains an update of the results published in Ref. [13]. Itonaga *et al*. introduced additional potentials, $\mathrm{V}_{2\pi/\rho}$ and $\mathrm{V}_{2\pi/\sigma}$, in which terms of correlated $2\pi/\rho$ and $2\pi/\sigma$ exchanges are taken into account [41] because it has a strong tensor force but still has opposite sign to that of the one-pion exchange potential. It was also pointed out that two-nucleon induced nonmesonic decay ($\Lambda NN \to NNN$) could play an important role in the nonmesonic weak decay [42]. However, no experiment has so far explicitly measured the contribution of the two-nucleon process.

The present results of the nonmesonic decay widths and the Γ_n/Γ_p ratios provide good criteria to test the short-range nature of the nonmesonic decay, which is essentially important to understand its mechanism. However, as shown in Fig. 10 and 11, there is no theoretical calculation that explains both the nonmesonic decay width and the Γ_n/Γ_p ratio consistently. For instance, the quark-current exchange model gives the Γ_n/Γ_p ratio in nuclear matter comparable to the present experimental data, but overestimates the nonmesonic decay width. The conventional meson exchange models, in which the contribution of heavy mesons are included, provide larger Γ_n/Γ_p ratios than those by the one-pion exchange model, though the results of meson exchange models are still smaller than the experimental data.

From an experimental point of view, more exclusive information, such as the angular correlation of outgoing nucleons and the detection of low-energy neutrons, would

also help to solve the puzzle of the Γ_n/Γ_p ratio. Recently, an experiment to measure the neutron spectra of the nonmesonic weak decay of ${}^{12}_{\Lambda}$C and ${}^{89}_{\Lambda}$Y was carried out at KEK [47,48]. The observed number of neutrons in ${}^{12}_{\Lambda}$C [49] was reported to be smaller than that expected from Refs. [33,36]. In addition, coincidence measurements of the decay particles, including neutrons from the s- and p-shell hypernuclei, ${}^{5}_{\Lambda}$He and ${}^{12}_{\Lambda}$C, were carried out at KEK [50,51], and the data analysis is underway. A study of the correlation of pair nucleons emitted in the nonmesonic weak decay with much greater statistics would help to completely understand the nucleon spectra and to reduce any ambiguity in the final state interaction.

V. CONCLUSION

In the present study, we measured the pion and proton energy spectra and extracted the π^- mesonic decay widths (Γ_{π^-}), the total nonmesonic decay widths (Γ_{nm}), and the Γ_n/Γ_p ratios on medium-to-heavy Λ hypernuclei with high precision. The results of Γ_{π^-} on ${}^{12}_{\Lambda}$C confirmed an increase of the mesonic decay width, which is interpreted as due to the distorted pion wave function and the nuclear shell-model configurations. The total nonmesonic decay widths (Γ_{nm}) in medium-to-heavy Λ hypernuclei almost saturates at $A \sim 56$. This suggests that the short-range nature and the local density approximation take central roles in the mechanism of the nonmesonic decay. The present Γ_n/Γ_p ratios are now comparable with the recent calculations based on the meson exchange potentials taking into account of heavy mesons such as kaon, ρ and ω and/or the quark current. Although the experimental uncertainty in deriving the Γ_n/Γ_p ratios become less than ever, the experimental Γ_n/Γ_p ratios are still larger than the theoretical calculations. At this moment, there is no theoretical calculation that can reproduce both the nonmesonic decay widths and the Γ_n/Γ_p ratios. Further experimental and theoretical efforts are needed to fully reveal the mechanism of the nonmesonic weak decay.

ACKNOWLEDGMENTS

The authors thank Professor K. Nakai and Professor T. Yamazaki for their continuous encouragement throughout the experiment from the beginning. We deeply appreciate the staff members of KEK and INS for their generous support to carry out the experiment and data analysis. Discussions with Professor K. Itonaga, Professor T. Motoba, Professor T. Fukuda, and Professor T. Nagae are greatly appreciated. One of the authors (H.B.) acknowledges partial support from the Korea-Japan collaborative research program of KOSEF (R01-2000-000-00019-0) and the Korea Research Foundation (2000-015-Dp0084).

[1] M. Danysz *et al*., Philos. Mag. **44**, 348 (1953).
[2] M. Ericson, Nucl. Phys. **A547**, 127cc (1992).
[3] H. Outa *et al*., Nucl. Phys. **A585**, 109c (1995).
[4] H. Outa *et al*., Nucl. Phys. **A639**, 251c (1998).
[5] J.J. Szymanski *et al*., Phys. Rev. C **43**, 849 (1991).
[6] A. Sakaguchi *et al*., Phys. Rev. C **43**, 73 (1991).
[7] H. Noumi *et al*., Phys. Rev. C **52**, 2936 (1995).
[8] T. Motoba *et al*., Nucl. Phys. **A489**, 683 (1988).
[9] T. Motoba and K Itonaga, Prog. Theo. Phys., Suppl. No. 117, 477 (1994).
[10] J. Nieves and E. Oset, Phys. Rev. C **47**, 1478 (1993).
[11] J.F. Dubach, Nucl. Phys. **A450**, 71c (1986).
[12] H. Bando, T. Motoba, and J. Zofka, Int. J. Mod. Phys. A **5**, 4021 (1990).
[13] A. Parreno, A Ramos, and C. Bennhold, Phys. Rev. C **56**, 339 (1997).
[14] K. Itonaga *et al*., Nucl. Phys. **A639**, 329c (1998).
[15] T. Inoue, S. Takeuchi, and M. Oka, Nucl. Phys. **A597**, 563 (1996).
[16] H. Bhang *et al*., Phys. Rev. Lett. **81**, 4321 (1998).
[17] H. Park *et al*., Phys. Rev. C **61**, 054004 (2000).
[18] O. Hashimoto *et al*., Phys. Rev. Lett. **88**, 042503 (2000).
[19] B. Povh, Nucl. Phys. **A335**, 233 (1980).
[20] K.H. Tanaka *et al*., Nucl. Instrum. Methods A **363**, 114 (1995).
[21] C.B. Dover *et al*., Phys. Rev. C **22**, 2073 (1980).
[22] T. Fukuda *et al*., Nucl. Instrum. Methods A **361**, 485 (1995).
[23] D.H. Davis, Nucl. Phys. **A547**, 369c (1992).
[24] T. Hasegawa *et al*., Phys. Rev. C **53**, 1210 (1996).
[25] M. Akei *et al*., Nucl. Phys. **A534**, 478 (1991).
[26] Y.D. Kim *et al*., Nucl. Instrum. Methods A **372**, 431 (1996).
[27] CERN Program Library Entry W **5013**, *GEANT*.
[28] T. Motoba *et al*., Phys. Rev. C **38**, 1322 (1988).
[29] G. Bohm *et al*., Nucl. Phys. **B24**, 248 (1970).
[30] M. Julic *et al*., Nucl. Phys. **B47**, 36 (1972).
[31] S. Ajimura *et al*., Phys. Rev. Lett. **68**, 2137 (1992)
[32] T. Kishimoto *et al*., Phys. Rev. C **51**, 2233 (1995)
[33] A. Ramos *et al*., Phys. Rev. C **55**, 735 (1997).
[34] A. Ramos (private communications).
[35] R.C. Carrasco *et al*., Nucl. Phys. **A570**, 701 (1994).
[36] A. Ramos *et al*., Preprint in nucl-th/0206036.
[37] J.A. Carr *et al*., Phys. Rev. C **25**, 952 (1982).
[38] C.S. Whisnant, Phys. Rev. C **34**, 262 (1986).
[39] H. Ohm *et al*., Phys. Rev. C **55**, 3062 (1997).
[40] P Kulessa *et al*., Nucl. Phys. **A639**. 283c (1998).
[41] K. Itonaga *et al*. Phys. Rev. C **65**, 034617 (2002).
[42] W.M. Alberico *et al*., Phys. Rev. C **61**, 044314 (2000).
[43] A. Ramos *et al*., Phys. Rev. C **50**, 2314 (1994).
[44] K. Sasaki *et al*., Nucl. Phys. **A669**, 331 (2000); **A678**, 455 (2000).
[45] A. Parreno and A Ramos, Phys. Rev. C **65**, 015204 (2001).
[46] W.M. Alberico, Nucl. Phys. **A691**, 163c (2001).
[47] KEK PS experiment E369, spokesperson T. Nagae (1996).
[48] H. Hotchi *et al*., Phys. Rev. C **64**, 044302 (2001).
[49] J.H. Kim *et al*., Phys. Rev. C **68**, 065201, (2003).
[50] KEK PS experiment E462, spokesperson H. Outa (2000).
[51] H.C. Bhang *et al*., Nucl. Phys. **A691**, 156c (2002).